RSC Advances

ROYAL SOCIETY OF CHEMISTRY

www.rsc.org/advances

Journal Name

ARTICLE

Facile Fabrication of Three-Dimensional Graphene Microspheres using β-Cyclodextrin Aggregates as substrates and their Application for Midecamycin Sensing

Received 00th January 20xx,
Accepted 00th January 20xx

DOI: 10.1039/x0xx00000x

www.rsc.org/

Xiaofei Zhu[a,b,†], Jingkun Xu[a,†], Xuemin Duan[a,*], Limin Lu[b,*], Kaixin Zhang[a], Yansha Gao[a], Liqi Dong[a], Hui Sun[a]

Three-dimensional (3D) graphene (GR) microspheres have been successfully prepared for the first time by a simple facile and green method using β-cyclodextrin aggregates (β-CDAs) as substrates, which could be easily obtained from concentrated aqueous solutions of β-CD. The synthesized 3D GR/β-CDAs composites have been characterized by scanning electron microscopy (SEM), transmission electron microscopy (TEM), UV/Vis spectroscopy, and Raman spectroscopy. A possible formation mechanism was discussed. The as-prepared 3D GR/β-CDAs microspheres provided multidimensional electron-transport pathways, and this has been exploited in an electrode material for the electrocatalytic oxidation of midecamycin (MD), a widely used macrolide antibiotic. Electrochemical results indicated that the as-prepared 3D GR/β-CDAs microspheres exhibited a higher electrocatalytic activity towards MD oxidation than 2D GR or β-CDAs, which could be mainly attributed to the improved electrical properties and large surface area of the composite and the high recognition and enrichment capability of β-CDAs. Under the optimal conditions, the peak currents on a 3D GR/β-CDAs microspheres-modified electrode increased linearly with the concentration of MD in the range 0.07–250 μM. The detection limit of MD reached 20 nM (S/N =3). The present method is promising for the synthesis of high-performance catalysts for sensors, fuel cells and gas-phase catalysis.

Introduction

MD is a 16-membered macrolide antibiotic that shows high antibacterial activity towards Gram bacteria. It has been widely used for therapy of upper and lower respiratory tract infections, tonsillitis, pneumonia, and so on.[1,2] Due to this widespread use in treatment of infectious disease, the determination of MD is important to optimize such therapy and to avoid toxic concentrations. Electrochemical method is widely used to detection tremendous of electro-activity drug molecules by reason of its simple, sensitive, fast and mild condition characteristics. Based on the electroactivity of MD, it has also been investigated and determined conveniently by electrochemical methods.[3-5] A key role played in electrochemical detection should be the modified electrode materials, which determines the sensitivity and speed of response to a large extent. Though electrochemical detection of MD using modified electrodes have been reported, such as multi-walled carbon nanotube modified gold electrode[6] and electrochemically reduced GR modified glassy carbon electrode,[7] the sensitivity and detection limit still become potential obstacles in practical applications. Therefore, development electrochemical method for detection of MD with improved performance based on novel composite modified GCE is significant.

Carbon nanomaterials have been considered attractive candidates for electrochemical applications because of their extraordinary physical properties and remarkable conductivities. Graphene (GR), which consists of atom-thick sheets of carbon packed in a two-dimensional (2D) honeycomb lattice, has drawn considerable attention from both the experimental and theoretical scientific communities owing to its unique nanostructure and variety of fascinating electrical, thermal and mechanical properties.[8] The applications of GR have been reported in various field such as nanocomposites,[9] batteries,[10] supercapacitors,[11] chemical sensors and biosensors.[12,13] However, due to inevitable aggregation between individual GR sheets driven by strong π-π interaction, the GR easily tend to form irreversible agglomerates or even restock to form graphite.[14] Aggregated GR films are usually characterized by small specific surface area, low conductivity, and poor durability. These disadvantages seriously limit the applications of GR and GR based materials in many fields. Recent years have witnessed different methods to prevent the aggregation of GR, including the introduction of guest materials to fabricate sandwich structure composites, the preparation of GR sheets with highly corrugated, and the controlled assembly or growth of 3D GR.[15-17] Among them,

[a] School of Pharmacy, Jiangxi Science and Technology Normal University, Nanchang 330013, PR China. E-mail: duanxuemin@126.com. Tel.: +86 791 83802632; Fax: +86 791 83805385
[b] College of Science, Jiangxi Agricultural University, Nanchang 330045, PR China. E-mail: lulimin816@hotmail.com
† These authors contributed equally to this work and should be considered co-first authors.
Electronic Supplementary Information (ESI) available: The optimization of supporting electrolyte, the optimization of solution pH and the relationship between solution pH and anodic peak potential. See DOI: 10.1039/x0xx00000x

3D-structured GR has been widely explored due to the following advantageous features. First, 3D GR exhibited higher conductivity as compare to 2D GR due to the absence of junction resistance of interface GR sheet.[18-20] Second, benefit from large number of wrinkles on its surface, 3D GR provided large surface area and abundant active sites, which were very suitable for decorating other electroactive material with high quality load level.[21] Third, the 3D structure promoted the access of analyte and electrolyte to the 3D GR electrode surface.

To date, a lot of methods have been developed to prepare 3D GR with different properties, structures and morphologies, including self-assembly[22] and template-assisted assembly[23]. Self-assembly has been confirmed as a powerful technique for constructing 3D GR architectures with hierarchical structures. Unfortunately, a freeze-drying process is necessary for the formation of 3D structures. While template-assisted assembly can prepare specific structure of 3D GR by adjusting the template structure,[24,25] but the relatively complicated experimental procedures and harsh experimental conditions have limited its wide application. Alternatively, assemble GO on templates followed by reduction is another effective method to obtained 3D GR.[17,26] However, these synthetic processes are hampered by the use of hazardous etchants such as HF/THF, and are often time-consuming and expensive. Therefore, it has remained a great challenge to fabricate desired 3D GR architectures through facile and green methods.

β-CD is an oligosaccharide which consist of seven glucose units, the inner cavity of toroidal shaped β-CD is hydrophobic while the exterior is hydrophilic. Previous reports have shown that β-CD in solution is bound together by a network of hydrogen bonds to form aggregates, and that the formation of such aggregates is related to solution pH whereas their size depends to some degree on the β-CD concentration.[27-30] Since β-CD had proved to be a good stabilizer and dispersing agent, especially for GR,[31-33] the utilization of β-CD to decorate materials to improve their performance became the most popular topic in the vast body of literature.[34-36] It is also interesting and worthy of study to assess the outcome of decorating β-CDAs on carbon materials. However, to the best of our knowledge, no literature exists on preparing 3D GR microspheres by using β-CDAs as substrates. In addition, as sensing materials, β-CDAs play a key role in signal amplification due to their high recognition and enrichment capabilities.

Our present work is concerned with the construction of 3D GR by using β-CDAs as substrates and investigation of its electrochemical performance. A stable suspension of β-CDAs was prepared based on the fact that β-CD molecules cross-link with each other through their hydroxyl groups and tend to form sphere-like structures under appropriate conditions. By virtue of the negatively charged groups on its surface, GO could be successfully assembled on the as-prepared β-CDA substrates through hydrogen bonding/van der Waals-type interactions. 3D GR/β-CDA microspheres were finally obtained after applying an electrochemical process to convert GO into GR. SEM, TEM, Raman spectroscopy, UV/Vis spectrophotometry, and electrochemical impedance spectroscopy were used to characterize the 3D GR/β-CDA microspheres. The as-prepared microspheres were very suitable for electrode materials in view of their large surface area, excellent electrical conductivity, strong enrichment capacity, and ability to capture target molecules. These excellent properties of the 3D GR/β-CDA microspheres permitted their use for the quantitative detection of MD over a wide range, with a low detection limit and no interference from common species.

Experimental

Chemicals and reagents

Midecamycin was purchased from Aldrich. Midecamycin stock solution (5×10^{-3} M) was prepared in absolute ethanol and stored at 277□281 K. GO was obtained from Nanjing Xianfeng nano Co. β-CD was purchased from the Beijing Chemical Reagent factory (Beijing, China). Lithium perchlorate trihydrate ($LiClO_4•3H_2O$), acetic acid, disodium hydrogenphosphate dodecahydrate (Na_2HPO_4), and sodium dihydrogenphosphate dehydrate (NaH_2PO_4) were obtained from Sinopharm chemical reagent Co. Ltd. Al reagents were of analytical grade unless specific instructions. Redistilled water was used during the experiments.

Instrumentation

SEM images were obtained with a Helios NanoLab FESEM/FIB instrument. TEM images were recorded using a Tecnai G2 F30 microscope. UV/Vis spectral analysis was performed using a Perkin-Elmer Lambda 900 ultraviolet-visible-near-infrared spectrophotometer (Germany). Raman spectroscopy (invia-reflex) was performed with a 633 nm laser. Electrochemical measurements were carried out on a CHI 660D electrochemical workstation (Shanghai, China). The measurement was carried out in a three-electrode system, including glass carbon electrode (GCE) or composites modified GCE as working electrode, platinum wire as auxiliary electrode and saturated calomel reference electrode (SCE). During the experiments, the atmosphere of redistilled water was set by passing N_2 for 15 min.

Material preparation

Synthesis of β-CDAs: β-CD (150 mg) was suspended in deionized water (10 mL). In order to avoid excessive precipitation, the suspension was adjusted to pH 5.5 by the addition of acetic acid. A solution of β-CDAs was obtained after vigorous stirring for 30 min at room temperature.

Synthesis of GO/β-CDAs: GO was dispersed in deionized water to obtain a concentration of 0.4 mg mL^{-1}, and this was subjected to ultrasonic treatment for 2 h. For comparison purposes, 0.1, 0.15, 0.25, 0.3, 0.6, and 0.9 mg mL^{-1} concentrations of GO were also prepared. The β-CDAs solution was then mixed with the GO dispersion to facilitate the assembly process.

Synthesis of 3D GR/β-CDAs microspheres-modified electrode: Before modification, glassy carbon electrode (GCE) was mechanically polished using chamois leather containing 0.05 μm Al_2O_3, and then it was ultrasonically cleaned with redistilled water, absolute ethanol and redistilled water, respectively, each for 5 min. The cleaned GCE was dried with a nitrogen stream prior to the subsequent modification. To obtain the 3D GR/β-CDAs microspheres-modified GCE, 5 μL of the GO/β-CDAs dispersion was dropped onto the surface of the GCE and dried at room temperature. The GO/β-CDAs/GCE was transferred to an electrochemical cell containing 0.1 M phosphate buffer solution (PBS) (pH 7.0). GO in GO/β-CDAs composite was electrochemically reduced to GR by performing successive voltammetric sweeps for 400 s with a potential window between -1.3 V to 0 V. Scan rate

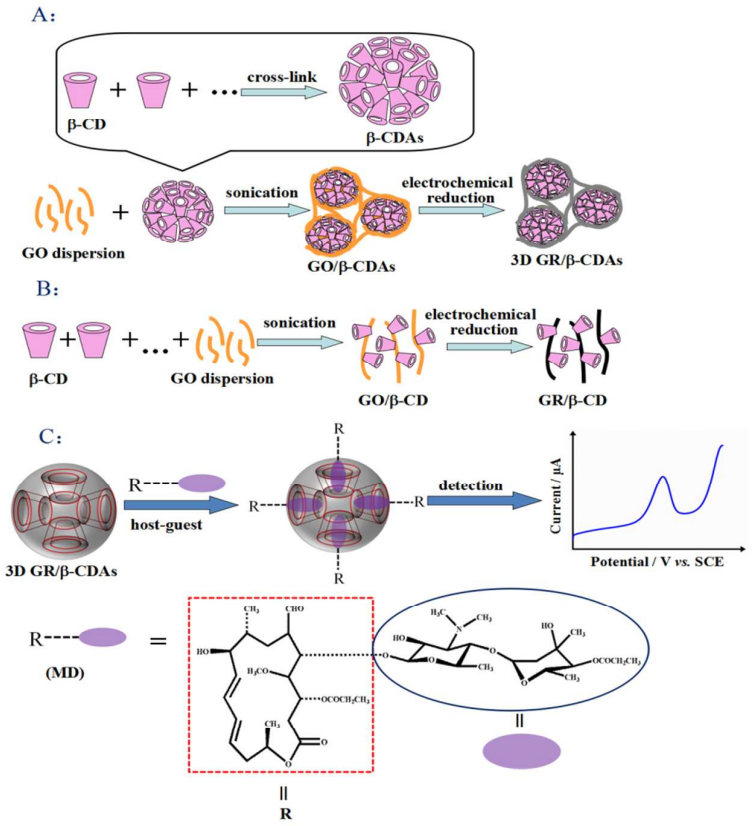

Scheme 1 (A) The preparation process of 3D GR/β-CDAs. (B) The preparation process of GR/β-CD. (C) The interaction between 3D GR/β-CDAs and MD.

was set as 50 mV s^{-1}. The resulting modified electrode was designated as 3D GR/β-CDAs/GCE.

For comparison, GR/GCE was prepared by a similar method without the introduction of β-CDAs. A GO-modified GCE (GO/GCE) and a β-CDAs-modified GCE (β-CDAs/GCE) were also prepared.

Results and discussion

The proposed formation mechanism of the described 3D GR/β-CDAs microspheres is shown in Scheme 1. The synthesis involved three main steps. The first step was the aggregation of β-CD. It is well established that β-CD is a basket-shaped molecule with a hydrophobic interior and hydrophilic exterior. Due to their exterior hydrophilic surface, β-CD molecules cross-link with each other through their hydroxyl groups, which ultimately leads to the formation of aggregates with a sphere-like structure.[37] In the second step, the obtained β-CDAs substrates were mixed with GO suspension. In this process, GO sheets assembled on the β-CDAs substrates by hydrogen bonding/van der Waals-type interactions. Finally, 3D GR/β-CDAs microspheres were obtained by electrochemical reduction to convert GO to GR. The prepared GR-based materials were characterized by SEM and TEM. From an SEM image (Fig. 1A), it can be observed that the surface morphology of GO/β-CDAs showed a typically wrinkled and crumpled structure, forming a rudiment of microsphere. While in Fig. 1B, GR-encapsulated β-CDAs spheres showed crinkled and rough textures due to the presence of flexible and ultrathin GR sheets, and the neighboring spheres were linked together by GR layers. A TEM image of 3D GR/β-CDAs (Fig. 1C) clearly revealed that GR sheets were wrapped around the surface of β-CDAs, forming a spherical structure. To our surprise, if the first step was omitted, that is, if β-CDs were directly added to a GO dispersion followed by electrochemical reduction (as shown in Scheme 1B), no 3D GR microspheres were formed. As can be seen from the SEM image (Fig. 1D), the product displayed a cracked morphology with a porous structure, indicating that the preparation process had an important effect on the morphology. This phenomenon might be due to the fact that β-CD molecules can be attached on the surface of GO through strong hydrogen-bonding/van der Waals forces and can then inhibit the formation of β-CDAs.

The obtained materials were characterized by Raman spectroscopy technique. A Raman spectrum usually features G and D bands, corresponding to sp^2 and sp^3 carbon stretching modes, respectively. Fig. 2A exhibits the Raman spectra of GO (a), GO/β-CDAs (b), and 3D GR/β-CDAs (c). It was found that the position and intensity of the D band did not change markedly, whereas the G band of GO at around 1579 cm^{-1} shifted to 1595 cm^{-1} for 3D GR/β-CDAs. This tendency can be ascribed to an increase in the number of sp3 carbon atoms on the GR during functionalization.[38] The D band at 1330 cm^{-1} gradually intensified, suggesting a reduction in the

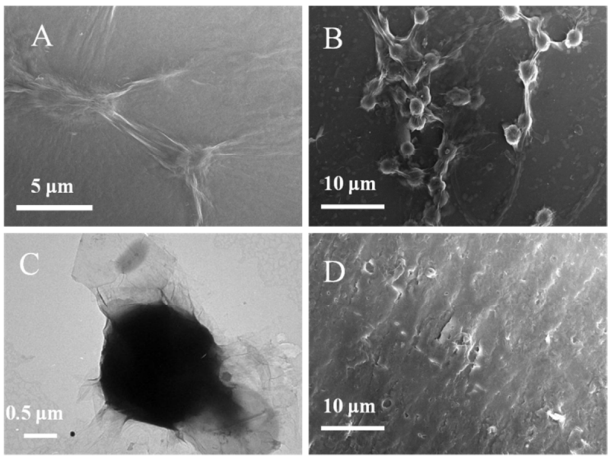

Fig. 1 (A) SEM of GO/β-CDAs. (B) SEM image of 3D GR/β-CDAs. (C) TEM image of 3D GR/β-CDAs. (D) SEM image of GR/β-CD.

size of the in-plane sp^2 domains.[39] The D/G band intensity ratio in the Raman spectrum expresses the atomic ratio of sp^2/sp^3 carbons, and is a measure of the extent of disordered graphite. As shown, a slightly increased D/G intensity ratio of GO/β-CDAs (1.07) relative to that of GO (1.01) was observed, which may have been due to the fact that the modified β-CDAs on the surface of GO existed in a disordered form.[40] For 3D GR/β-CDAs, the D/G intensity ratio (1.2) was higher than for either GO or β-CDAs/GO, which was attributed to the decrease of sp^2 domains average size during the reduction process.[41,42] These Raman spectroscopic results suggest a strong interaction between β-CDAs molecules and GO, and confirm the formation of 3D GR/β-CDAs after the electrochemical reduction process.

The nature of the obtained composite was further confirmed by its UV/Vis absorption spectrum. Fig. 2B displays the UV/Vis absorption spectra of GO/β-CDAs and 3D GR/β-CDAs. As can be seen, the characteristic absorption peak of GO/β-CDAs appears at 231 nm and corresponds to a π-π^* electron transition of the benzene ring. A shoulder peak at 303 nm might be associated with an $n\rightarrow\pi^*$ electron transition. The characteristic absorption peak of 3D GR/β-CDAs appeared at 245 nm. The shift of the peak from 231 to 245 nm suggested that the GO/β-CDAs had been successfully reduced to 3D GR/β-CDAs.[43]

Electrochemical impedance spectroscopy (EIS) is a useful technique to characterization of surface modified electrode.[44] Impedance spectrum usually includes a semicircle part and a linear part, the semicircle part at high frequencies corresponding to electron transfer resistance (R_{et}) while the linear part at low frequencies corresponding to diffusion process. Fig. 2C shows the results of EIS on bare GCE (curve a), GO/GCE (b), GR/GCE (curve c), and 3D GR/β-CDAs/GCE (curve d) in the presence of 0.1 M KCl containing 5 mM $[Fe(CN)_6]^{3-/4-}$ obtained at a scan rate of 0.05 V s^{-1}. As can be seen, R_{ct} of the bare GCE was 445 Ω. While GO/GCE displayed an R_{ct} of 4150 Ω due to the poor conductivity of GO. When the surface of the GCE was modified with 2D GR, the R_{ct} value decreased dramatically, which can be attributed to the excellent electronic property of 2D GR, forming a fast electron conduction pathway between GCE and the electrochemical probe. For 3D GR/β-CDAs/GCE, however, the Ret was significantly increased to 1070 Ω, larger than that of 3D GR/GCE. Possibly due to the non-conducting β-CDAs molecules loaded on the surface of the 3D GR and impede interfacial charge transfer.

The electrochemical behavior of MD at different modified GCEs was studied by cyclic voltammetry. Fig. 3A presents typical cyclic voltammograms of the GO/GCE (inset in Fig. 3A, curve a), β-CDAs/GCE (inset in Fig. 3A, curve b), bare GCE (curve c), GR/GCE (Fig. 3A, curve d), and 3D GR/β-CDAs/GCE (Fig. 3A, curve e) in pH 7.0 PBS containing 20 μM MD. At the bare GCE and GO/GCE, no obvious redox peak could be seen within the potential window from 0.3 to 0.8 V, which may have been due to the sluggish electron transfer of the bare GCE and poor conductivity of GO. β-CDAs/GCE exhibited a distinct oxidation peak current response (curve b), which might be attributed to the fact that β-CDAs have good host–guest recognition and enrichment

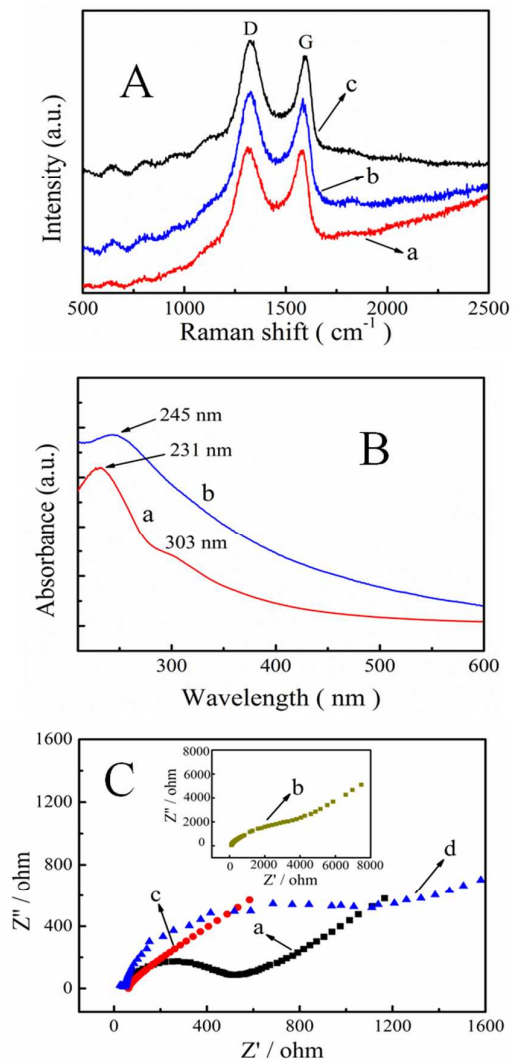

Fig. 2 (A) Raman spectra of GO (a), GO/β-CD (b), and 3D GR/β-CDAs (c). (B) UV/Vis absorption spectra of GO/β-CD (a) and 3D GR/β-CDAs (b). (C) Impedance spectra of GCE (a), GO/GCE (b), GR/GCE (c), and 3D GR/β-CDAs/GCE (d) in 5 mM $Fe(CN)_6^{3-/4-}$ (1:1) solution containing 0.1 M KCl.

properties but also exhibit poor conductivity.[45] At 2D GR/GCE (curve d), the oxidation peak current as well as the background current increased significantly due to the excellent electrical conductivity and large surface area of 2D GR.[46,47]

Moreover, the oxidation peak current increased further on the 3D GR/β-CDAs/GCE (curve e). Indeed, the oxidation peak current of MD at the 3D GR/β-CDAs/GCE was about 8 times larger than that at 2D GR/GCE, which demonstrated that 3D GR/β-CDAs had a greater electrocatalytic property for MD. The observed oxidation peak with higher current response could be attributed to the fact that 3D sphere-like GR/β-CDAs have abundant accessible active sites that can effectively interface with electrolytes, facilitate electron transfer, and provide multiplexed and highly conductive pathways.[48] In addition, the β-CDAs in the 3D GR/β-CDAs composite with high supramolecular recognition capability can form inclusion complexes with MD (Scheme 1C). The host guest inclusion action can further enhance the accumulation effect of 3D GR/β-CDAs and thus increase the MD concentration on the surface of electrode, leading to a pronounced peak current.

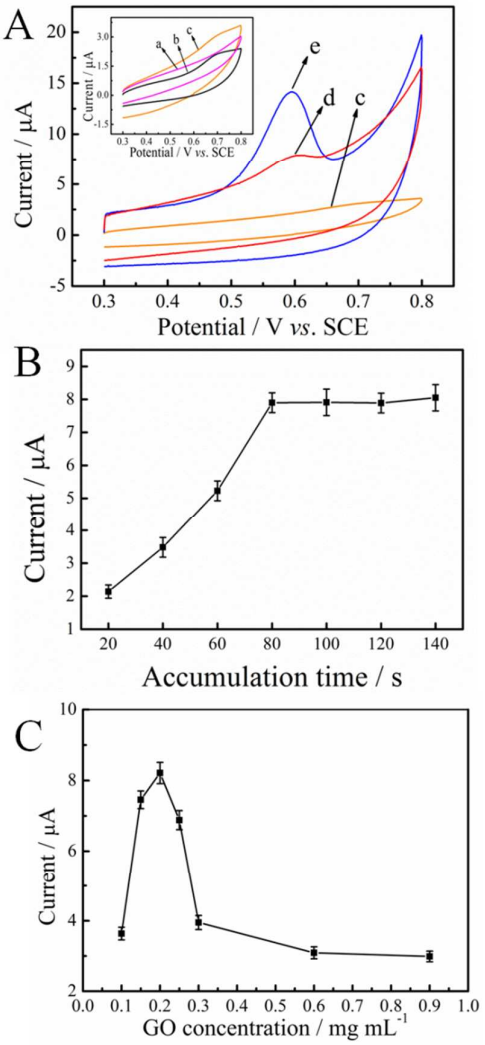

Fig. 3 (A) Cyclic voltammograms of 20 μM MD in 0.1 M PBS (pH 7.0) at GO/GCE (a), β-CDAs/GCE (b), bare GCE (c), GR/GCE (d), and 3D GR/β-CDAs/GCE (e). Accumulation time: 80 s. Scan rate: 50 mV s^{-1}. (B) Variation of the peak current with accumulation time in 0.1 M PBS (pH 7.0). MD concentration: 10 μM. Scan rate: 50 mV s^{-1}. (C) Influence of different concentrations of GO (0.1 mg mL^{-1}, 0.15 mg mL^{-1}, 0.2 mg mL^{-1}, 0.25 mg mL^{-1}, 0.3 mg mL^{-1}, 0.6 mg mL^{-1}, and 0.9 mg mL^{-1}) on the oxidation peak current of 10 μM MD.

Since accumulation time leads to more MD being absorbed on the electrode surface, and hence improves the determination sensitivity, it was necessary to investigate the influence of accumulation time. As can be seen in Fig. 3B, the peak current of MD increased with the accumulation time and reached a maximum at 80 s. This indicated that accumulation for 80 s led to saturated adsorption of MD on the 3D GR/β-CDAs/GCE. Considering both sensitivity and work efficiency, 80 s was employed in further experiments. Fig. 3C shows the changes in the peak current at different concentrations of GO when the concentration of β-CDAs was fixed at 4 mg mL^{-1}. Clearly, the oxidation peak current of MD increased with the increasing of GO concentrations from 0 to 0.2 mg mL^{-1}, which was due to the fact that the increasing of GO concentrations can increase the conductivity of the obtained GR/β-CDAs composite. However, the oxidation peak current of MD decreased gradually from 0.2 to 0.9 mg mL^{-1}, which can be ascribed the fact too much GO could result in an aggregation of GR sheets on the surface of β-CDAs and hindered the electrochemical performance. Therefore, a dispersion of GO/β-CDAs hybrid containing 0.2 mg mL^{-1} GO and 4 mg mL^{-1} β-CD was used to modify the GCE. Furthermore, the influence of buffer solutions on the electrooxidation response at 3D GR/β-CDAs/GCE (Fig. S1) was investigated in $LiClO_4$, KCl, Na_2CO_3, PBS, NH_4Cl, and $NaHCO_3$ buffer solutions, all of which contained 10 μM MD. MD showed slight voltammetric responses in $LiClO_4$ and KCl buffer solutions, whereas its obvious oxidation peak could be observed in Na_2CO_3, PBS, NH_4Cl, and $NaHCO_3$ buffer solutions. However, the maximum current response was obtained in PBS. Thus, PBS was used to investigate the electrochemical behavior of MD and detection of its content in the following experiments.

The effect of pH on the sensing properties of 3D GR/β-CDAs/GCE was carefully investigated with 20 μM MD in the pH range from 6.0 to 9.0 in PBS (0.1 M) at a scan rate of 50 mV s^{-1} (Fig. S2a). As can be seen, with the increasing of solution pH, the oxidation potential (E_{pa}) of MD shifted toward negative values. The dependence of E_{pa} on the pH can be represented as E_{pa} = 0.961 – 0.049 pH with R^2 = 0.990 (Fig.S2b). A slope of -49 mV pH^{-1} indicating electrode reaction involved the same number of electrons and protons. Simultaneously, it was also found that the oxidation peak exhibited highest current when the pH value was 7.0. Therefore, the pH value of PBS was set as 7.0 for further experiment.

The effect of scan rate on the electrochemical oxidation of MD at the 3D GR/β-CDAs/GCE was investigated by CV for the purpose of understanding its electrochemical mechanism. As shown, with the increase of scan rate, the peak current increased as well (Fig. 4A), linearly with the scan rate from 10 to 400 mV s^{-1}. The linear equation was I (μA) = 1.941 + 0.094 v (R^2 = 0.996) (insert of Fig. 3A), indicating that electro-oxidation of MD on 3D GR/β-CDAs/GCE was a adsorption-controlled process.[49] Similarly, a linear relationship between E_{pa} and the natural logarithm of v (ln v) was also

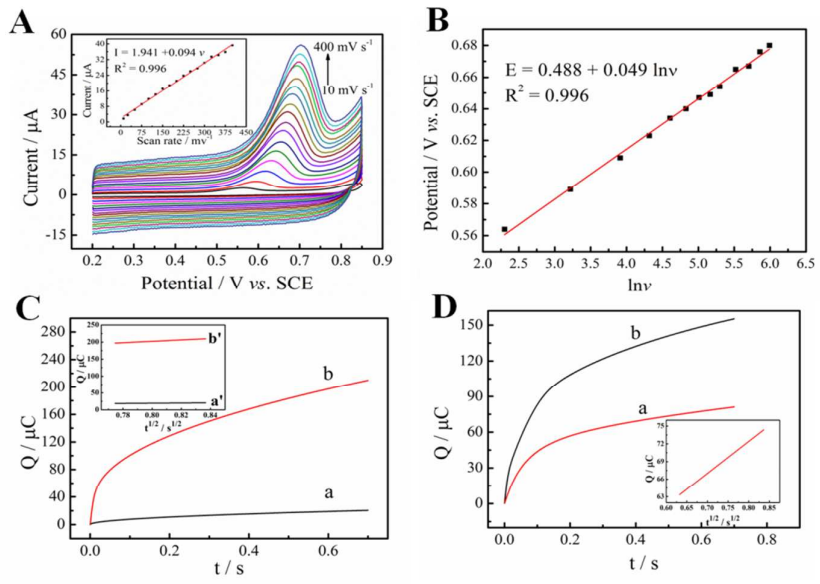

Fig. 4 (A) Cyclic voltammograms of 20 μM MD with different scan rates (v) on 3D GR/β-CDAs/GCE in 0.1 M PBS (pH 7.0) (from the inner to the outer are 10, 25, 50, 75, 100, 125, 150, 175, 200, 225, 250, 275, 300, 325, 350, 375 and 400 mV s^{-1}, respectively.). Accumulation time: 80 s. Insert: linear relationship of anodic peak current I versus v. (B) The relationship between E_p and logarithm of v. (C) Plot of Q-t curves of bare GCE (a) and 3D GR/β-CDAs/GCE (b) in 0.1 mM $K_3[Fe(CN)_6]$ containing 1.0 M KCl. Insert: Plot of Q-$t^{1/2}$ curves on bare GCE (a´) and 3D GR/β-CDAs/GCE (b´). (D) Plot of Q-t curves of 3D GR/β-CDAs/GCE in 0.1 M PBS (pH 7.0) in the absence (a) and presence (b) of 0.5 mM MD. Insert: plot of Q–$t^{1/2}$ curve after background subtraction.

observed in the range 10-400 mV s^{-1} (Fig. 4B), and the linear regression equation can be expressed as $E_{pa} = 0.488 + 0.049 \ln v$ ($R^2 = 0.996$). For fully irreversible and adsorption-controlled electrode process, E_{pa} can be expressed as:[50]

$$E_{pa} = E^0 + (RT/\alpha nF) \ln (RTk^0/\alpha nF) + (RT/\alpha nF) \ln v$$

where E^0 is the formal redox potential, α is the transfer coefficient, n is the number of electrons transferred in the rate-determining step, k^0 is the standard rate constant of the reaction, v is the scan rate, R is the gas constant, T is the absolute temperature, and F is the Faraday constant. Accordingly, the slope of a straight line of a plot of E_{pa} against ln v is equal to RT/αnF, and the value of αn was calculated as 0.53. Generally, α is assumed to be 0.5 in a fully irreversible electrode process,[49] therefore the electron transfer number (n) is around 1. Considering the equal number of electrons and protons involved in the electro-oxidation of MD as demonstrated above, the electrooxidation of MD at 3D GR/β-CDAs/GCE is a one- proton and one-electron process. The standard heterogeneous rate constant (k_s) can also be obtained according to the following equation:[51]

$$k_s = 2.415 \exp(-0.02\ F/RT)\ D^{1/2} (E_{pa} - E_{pa/2})^{-1/2} v^{1/2}$$

where $E_{pa/2}$ represents the potential at which $I = I_{pa/2}$, v is the scan rate, and D is the diffusion coefficient, determined by chronocoulometry as described below. Based on these experimental results and salient literature reports,[5,6,52] a possible redox mechanism of MD on the 3D GR/β-CDAs/GCE is proposed as shown in Scheme 2. The electrochemically effective surface areas (A) of 3D GR/β-CDAs/GCE and bare GCE were determined by chronocoulometry using 0.1 mM $K_3Fe(CN)_6$ containing 1 M KCl (Fig. 4C) based on the Anson equation:[53]

$$Q(t) = 2nFAcD_0^{1/2}t^{1/2}/\pi^{1/2} + Q_{dl} + Q_{ads}$$

where Q_{ads} is the Faradic charge, Q_{dl} is the double-layer charge, D_0 is the diffusion coefficient (the diffusion coefficient of $K_3[Fe(CN)_6]$ in 1 M KCl is 7.6×10^{-6} cm^2 s^{-1}),[54] c is the concentration of the substrate, and A is the surface area of the working electrode. Other symbols have their usual meanings. The linear regression equation of Q-$t^{1/2}$ curves on bare GCE (a') and 3D GR/β-CDAs/GCE (b') were Q (10^{-6} C) = – 0.319 + 18.121 $t^{1/2}$ ($R^2 = 0.999$) and Q (10^{-6} C) = 38.431 + 204.940 $t^{1/2}$ ($R^2 = 0.999$) (inset in Fig. 4C). Based on the slopes of the linear relationship between Q and $t^{1/2}$, A was calculated as 0.682 cm^2 for 3D GR/β-CDAs/GCE, which is over ten times that for bare GCE (0.060 cm^2). The results indicated that the effective surface area of the electrode was obviously increased after modification, which could increase the number of electrochemically active sites, enhance the electrochemical response, and decrease the detection limit.

Chronocoulometry was further carried out in 0.1 M PBS (pH 7.0) in the absence and presence of 0.5 mM MD (Fig. 4D).

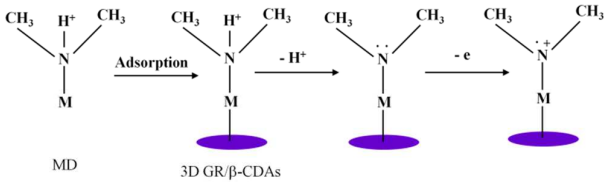

Scheme 2 Electrochemical oxidation mechanism of MD.

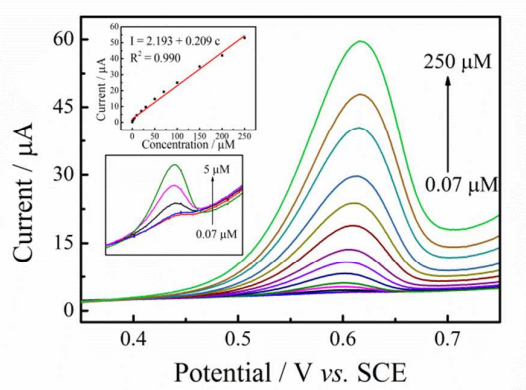

Fig. 5 Linear sweep voltammetrys of 0.07, 0.09, 0.2, 2, 5, 10, 20, 30, 50, 70, 100, 150, 200 and 250 μM MD on 3D GR/β-CDAs/GCE in 0.1 M PBS (pH 7.0) at the scan rate of 50 mV s^{-1}. Insert: plot of the oxidation peak current against the concentration of MD.

As can be seen in the inset in Fig. 4D, a plot of Q versus $t^{1/2}$ shows a linear relationship after background subtraction, with an equation of Q (μC) = 29.103 + 54.124 $t^{1/2}$ (R^2 = 0.999); the intercept (Q_{ads}) is 2.910 × 10^{-5} C and the slope is 5.412 × 10^{-5} C $s^{-1/2}$. As n = 1, A = 0.682 cm^2, and c = 0.5 mM, D was calculated to be 2.11 × 10^{-4} cm^2 s^{-1}. According to the equation Q_{ads} = nAFΓ_s, the adsorption capacity (Γ_s) was calculated as 4.42 × 10^{-10} mol cm^{-2}, and k_s for MD was thus calculated to be about 4.43 × 10^{-2} cm s^{-1}.

Under the optimal experimental conditions established above, the calibration curves of MD in PBS were measured by linear sweep voltammetry (LSV). Fig. 5 shows representative LSV traces of different concentrations of MD in pH 7.0 PBS. As can be seen, the oxidation peak current was positive correlation to the MD concentration in the range 0.07–250 μM. The regression equation was I = 2.193 + 0.209 c (R^2 = 0.990). The detection limit for MD was estimated to be 20 nM (S/N = 3). Additionally, the efficiencies of the 3D GR/β-CDAs/GCE and other modified electrodes for MD determination are compared in Table 1. It can be seen that 3D GR/β-CDAs/GCE was more sensitive, with a wider linear range and lower detection limit. These comparison data further indicate that 3D GR/β-CDAs/GCE exhibited very high electrochemical performance toward MD.

Table 1
Comparison of MD detection for the reported electrochemical sensors.

Type of electrode	Linear range (μM)	Detection limit (μM)	Reference
[a]MWCNT/GCE	0.5–20	–	[45]
Au electrode	207.99–404.06[b]	–	[46]
GCE	2.46–61.43[c]	1.23	[47]
3D GR/β-CDAs/GCE	0.07–250	0.02	This work

[a] Multi-walled carbon nanotube
[b] The linear range in literature [46] is 0.1693–0.3289 mg mL^{-1}, equal to 207.99–404.06 μM.
[c] The linear range in literature [47] is 2–50 μg mL^{-1}, equal to 2.46–61.43 μM.

Table 2
Recovery measurements of the MD in the urine samples using the modified electrode.

Samples	Added (μM)	Found (μM)	*RSD (%)	Recovery (%)
1	0	0	–	–
2	0.09	0.0873	1.89	97.00
3	0.22	0.216	2.22	98.18
4	0.96	0.973	2.54	101.35
5	4.3	4.401	3.83	102.34
6	9.8	9.782	2.87	99.81

* RSD (%) calculated from five separate experiments.

The reproducibility of the proposed electrochemical sensor was evaluated by repeating the determination of 20 μM MD using eight modified electrodes, which gave a satisfactory relative standard deviation (RSD) of 3.9 %, indicating acceptable reproducibility and precision. To evaluate the long-term stability of 3D GR/β-CDAs/GCE, it was stored in air and used to detect 20 μM MD daily over a period of 4 weeks. Results indicate that after 4 weeks, the current response almost no obvious change compared with the original electrode, showing the 3D GR/β-CDAs/GCE to be quite stable. In addition, possible interferences were investigated by introducting other species while the MD concentration was fixed to 1 μM. We found that 50-fold concentrations of K^+, Ca^{2+}, Mg^{2+}, Na^+, Al^{3+}, Zn^{2+}, Pb^{2+}, NO_3^-, SO_4^{2-}, Fe^{3+}, Ag^+, or Cl^-, 30-fold concentrations of glucose, uric acid, oxalic acid, lactose, or tartaric acid, and 10-fold concentrations of vitamin B_1, vitamin B_2, or vitamin C in the solution did not interfere with the detection, the peak current changes being less than ± 5 %. The results indicate that this method has acceptable selectivity for the determination of MD.

Furthermore, the proposed sensor was applied to the determination of MD in urine samples. Urine samples were obtained from health volunteers, which were diluted 50-fold with 0.1 M PBS (pH 7.0) and centrifuged at 5000 rpm for 5 min to remove the suspended particles. Recovery test method was used to detect MD in urine samples by adding known amounts of MD. Percentage recovery and RSD date were determined and are presented in Table 2. As can be seen, the recovery of MD was in the range 97–102.34 %, indicating that the proposed method can be successfully applied for the detection of MD concentration in urine samples.

Conclusions

In summary, 3D GR/β-CDAs microspheres have been prepared by a facile preparation strategy based on electrochemical techniques with β-CDAs as substrates. The as-synthesized 3D GR/β-CDAs microspheres exhibited excellent electronic conductivity, large specific surface area, and fast apparent heterogeneous electron transfer, making them suitable for use as an excellent sensing platform for highly

sensitive determination of MD. Under optimized conditions, a 3D GR/β-CDAs microspheres-modified GCE exhibited good performance in terms of low limit of detection (20 nM) and wide linear range (0.07–250 μM). Moreover, it also exhibited good reproducibility, stability, and anti-interference ability. The success of this method suggests that 3D GR/β-CDAs microspheres may be developed as efficient and versatile high-performance electrocatalysts for electrochemical sensor applications.

Acknowledgements

We are grateful to the National Natural Science Foundation of China (51302117 and 51272096), the Natural Science Foundation of Jiangxi Province (20122BAB216011 and 20151BAB203018), Postdoctoral Science Foundation of China (2014M551857 and 2015T80688) and Postdoctoral Science Foundation of Jiangxi Province (2014KY14), Jiangxi Provincial Department of Education (GJJ13258) and the Science and Technology Landing Plan of Universities in Jiangxi province (KJLD12081 and KJLD14069) for their financial support of this work.

Notes and references

1 S. Alvarez-Elcoro and J. D. C. Yao, Macrolide antibiotics, second ed., Amsterdam, 2003.
2 K. Long, Handbook of clinical pharmaceutics, Gold Shield Press, Beijing, 1992.
3 R. Fan, F. Ji, J. Qian, Q. Wu, C. Bian, Y. Yang, *Acta Pharmaceutica sinica*, 1995, **30**, 34.
4 D. Liu, W. Jin, *J. Chromatogr. B.*, 2003, **783**, 509.
5 K. M. Drljević-Djurić, M. L. Avramov, S. D. Petrović, D. Z. Mijin, M. B. Jadranin, *Russ. J. Electrochem.*, 2011, **47**, 781.
6 H. Wan, F. Zhao, B. Zeng, *Colloid. Surface. B.*, 2011, **86**, 247.
7 X. Xi, L. Ming, *Anal. Methods*, 2012, **4**, 3013.
8 C. N. R. Rao, A. K. Sood, K. S. Subrahmanyam, A. Govindaraj, *Angew. Chem. Int. Ed.*, 2009, **48**, 7752.
9 J. Oh, J. H. Lee, J. C. Koo, H. R. Choi, Y. Lee, T. Kim, N. D. Luong, J. D. Nam, *J. Mater. Chem.*, 2010, **20**, 9200.
10 E. Yoo, J. Kim, E. Hosono, H. S. Zhou, T. Kudo, I. Honma, *Nano Lett.*, 2008, **8**, 2277.
11 S. Chen, J. Zhu, X. Wu, Q. Han and X. Wang, *ACS Nano*, 2010, **4**, 2822.
12 Y. Wang, Y. M. Li, L. H. Tang, J. Lu, J. H. Li, *Electrochem. Commun.*, 2009, **11**, 889.
13 Z. Wang, S. N. Liu, P. Wu, C. X. Cai, *Anal. Chem.*, 2009, **81**,1638.
14 J. S. Lee, S. I. Kim, J. C. Yoon, J. H. Jang, *ACS Nano*, 2013, **7**, 6047.
15 C. Z. Zhu, S. J. Guo, Y. M. Zhai, S. J. Dong. *Langmuir*, 2010, **26**, 7614.
16 J. Yan, J. P. Liu, Z. J. Fan, T. Wei, L. J. Zhang, *Carbon*, 2012, **50**, 2179.
17 S. Nardecchia, D. Carriazo, M. L. Ferrer, M. C. Gutiérrez, F. D. Monte, *Chem. Soc. Rev.*, 2013, **42**, 794.
18 X. Cao, Z. Zeng, W. Shi, P. Yep, Q. Yan, H. Zhang, *Small*, 2013, **9**, 1703.
19 X. Dong, Y. Cao, J. Wang, M. B. Chan-Park, L. Wang, W. Huang, P. Chen, *RSC Adv.*, 2012, **2** 4364.
20 X. Dong, J. Wang, J. Wang, M. B. Chan-Park, X. Li, L. Wang, W. Huang, P. Chen, *Mater. Chem. Phys.*, 2012, **134**, 576
21 X. Huang, X. Y. Qi, F. Boey and H. Zhang, *Chem. Soc. Rev.*, 2012, **41**, 666.
22 F. Liu, S. Y. Chung, G. Oh, T. E. Seo, *ACS Appl. Mater. Interfaces*, 2012, **4**, 922.
23 X. Cao, Z. Yin, H. Zhang, *Energ. Environ. Sci.*, 2014, **7**, 1850.
24 Z. P. Chen, W. C. Ren, L. B. Gao, B. L. Liu, S. F. Pei, H. M. Cheng, *Nat. Mater.*, 2011, **10**, 424
25 X. Cao, Y. Shi, W. Shi, G. Lu, X. Huang, Q. Yan, Q. Zhang, H. Zhang, *Small*, 2011, **7**, 3163.
26 J. C. Yoon, J. S. Lee, S. I. Kim, K. H. Kim, J. H. Jang, *Sci. Rep.*, 2013, **3**, 1788.
27 A. W. Coleman, I. Nicolis, N. Keller, P. D. Jean, *J. Incl. Phenom. Macro.*, 1992, **13**, 139.
28 X. Xiao, R. Liu, C. Qiu, D. Zhu, F. Liu, *Mat. Sci. Eng. C,* 2009, **29**,785.
29 G. González-Gaitano, P. Rodríguez, J. R. Isasi, M. Fuentes, G. Tardajos, M. Sánchez, *J. Incl. Phenom. Macro.*, 2002, **44**, 101.
30 T. Loftsson, M. Másson, M. E. Brewster, *J. Pharm. Sci.*, 2004, **93**, 1091.
31 Y. J. Guo, S. J. Guo, J. T. Ren, Y. M. Zhai, S. J. Dong, E. K. Wang, *ACS Nano*, 2010, **4**, 4001.
32 B. Konkena, S. Vasudevan, *Langmuir*, 2012, **28**, 12432.
33 L. Tan, K. G. Zhou, Y. H. Zhang, H. X. Wang, Y. F. Guo, H. L. Zhang, *Electrochem. Commun.*, 2010, **12**, 557.
34 G. B. Zhu, Y. H. Yi, H. Sun, K. Wang, Z. X. Han, X. Y. Wu, *J. Mater. Chem.*, 2015, **3**, 45.
35 Y. Gao, L. Wu, K. Zhang, J. Xu, L. Lu, X. Zhu, Y. Wu, *Chinese Chem. Lett.*, 2015, **26**, 613.
36 G. Wenz, *Angew. Chem. Int. Ed. Engl*, 1994, **33**, 803.
37 X. Xiao, R. Liu, C. Qiu, D. Zhu, F. Liu, *Mat. Sci. Eng. C*, 2009, **29**, 785.
38 C. H. Xu, J. C. Wang, L. Wan, J. J. Lin, X. B. Wang, *J. Mater. Chem.*, 2011, **21**, 10463.
39 H. Wang, J. T. Robinson, X. Li, H. Dai, *J. Am. Chem. Soc.*, 2009, **131**, 9910.
40 W. Song, J. Hu, Y. Zhao, D. Shao, J. Li, *RSC Adv.*, 2013, **3**, 9514.
41 A. C. Ferrari, J. Robertson, *Phys. Rev. B*, 2000, **61**, 14095.
42 S. Stankovich, D. A. Dikin, R. D. Piner , K. A. Kohlhaas, A. Kleinhammes, Y. Jia, Y. Wu, S. T. Nguyen, R. S. Ruoff, *Carbon*, 2007, **45**, 1558.
43 D. Li, M. Muller, S. Gilje, R. Kaner, G. Wallace, *Nat. Nanotechnol.*, 2008, **3**, 101.
44 Y. H. Liao, R. Yuan, Y. Chai, Y. Zhuo, X. Yang, *Anal. Biochem.*, 2010, **402**, 47.
45 S. Xiong, J. Cheng, L. He, M. Wang, X. Zhang, Z. Wu, *Anal. Methods*, 2014, **6**, 1736.
46 S. Stankovich, D. A. Dikin, G. H. B. Dommett, K. M. Kohlhaas, E. J. Zimney, E. A. Stach, R. D. Piner, S. T. Nguyen and R. S. Ruoff, *Nature*, 2006, **442**, 282.
47 M. Pumera, A. Ambrosi, A. Bonanni, E. L. K. Chng and H. L. Poh, *Trac-Trend Anal. Chem.*, 2010, **29**, 954.
48 X. Liu, J. S. Cui, J. B. Sun and X. T. Zhang, *RSC Adv.*, 2014, **4**, 22601.
49 A. J. Bard and L. R. Faulkner, Electrochemical methods: fundamentals applications, second ed., Wiley, New York, 1980.
50 E. Laviron, *J. Electroanal. Chem.*, 1974, **52**, 355.
51 J. G. Velasco, *Electroanal.*, 1997, **9**, 880.
52 N. Li, H. Luo and G. Chen, *Anal. Bioanal. Chem.*, 2004, **380**, 908.
53 F. Anson, *Anal. Chem.*, 1964, **36**, 932.
54 R. N. Adams, Electrochemistry at solid electrodes, Marcel Dekker, New York, 1969.